Pure Appl. Chem., Vol. 74, No. 9, pp. 1651–1661, 2002.

Formation of interfacial phases in the epitaxial growth of Sb on Si(111)-7 × 7 reconstructed surface*

Vinod Kumar Paliwal[1,2], A. G. Vedeshwar[2], and S. M. Shivaprasad[1,‡]

[1]*Surface Physics Group, National Physical Laboratory, New Delhi 110 012, India;*
[2]*Department of Physics and Astrophysics, University of Delhi, Delhi 110 007, India*

Abstract: Understanding the evolution of the Sb/Si(111) interface is of great interest in the formation of devices of nanodimensions. We have undertaken in situ (~10^{-11} torr) studies of Sb adsorption (at room temperature) and its desorption on the 7 × 7 reconstructed Si(111) surface, by complementary techniques such as X-ray photoelectron spectroscopy (XPS), Auger electron spectroscopy (AES), low-energy electron diffraction (LEED), and electron energy loss spectroscopy (EELS). For room-temperature (RT) Sb adsorption, the overlayer grows in the Frank van der Merwe mode, forming an interface state of δ(7 × 7) in the submonolayer Sb coverage regime. Adsorption of 1.0 monolayer (ML) Sb at RT shows an abrupt shift of 0.8 eV in the peak position of the Sb $3d_{5/2}$ transition owing to band-bending caused by a metallic (7 × 7) to a semiconducting (1 × 1) surface phase transformation. Changes observed in full width at half-maximum (fwhm) and Sb $3d_{3/2}$ and $3d_{5/2}$ branching ratio are discussed. Thermal annealing experiments provide evidence for agglomeration of Sb islands, before the multilayer and monolayer desorption. During this desorption process, we have observed two novel surface phases of (5 × 5) at 0.4 ML and ($5\sqrt{3} \times 5\sqrt{3}$ – R30°) at 0.2 ML, stable at higher temperatures.

INTRODUCTION

Formation of compositional and doping superlattices of nanodimensions enable the tailoring of advanced materials with novel properties, owing to the domination of quantum effects over the free-carrier distribution in this size regime [1,2]. Modern growth techniques such as molecular beam epitaxy (MBE) have enabled the formation of superlattices of monolayer dimensions and, thus, the practical realization of introducing artificial periodicity and, consequently, the band structure in a desired way, an example of which is the formation of δ-doped silicon structures. Since this process involves the formation of a dopant layer sandwiched between the silicon layers, the study of metal layer growth on single-crystal silicon surfaces has assumed importance. Such studies also address the issue of band-bending and Schottky barrier formation that are dependent on surface and interface states. The properties of metal/semiconductor interfaces have been a topic of great technological interest and scientific challenge over several decades. Multidirectional approaches to understand the deviations from the Schottky–Mott rule have yielded novel results, aiding the understanding at the atomistic level. It is now clear that apart from just metal-induced gap states (MIGS), there are other factors involved at the real metal/semiconductor contact, such as defect densities, growth kinetics, and interfacial strain. Since the kinetics of formation plays a dominant role in determining the interface and overlayer characteristics, a surface sci-

Pure Appl. Chem.* **74, 1489–1783 (2002). An issue of reviews and research papers based on lectures presented at the 2nd IUPAC Workshop on Advanced Materials (WAM II), Bangalore, India, 13–16 February 2002, on the theme of nanostructured advanced materials.
‡Corresponding author: Fax: +91-11-5852678; E-mail: prasad@csnpl.ren.nic.in

ence approach to such studies is imperative. Thus, there are several studies in the literature that are directed toward understanding the initial stages of formation of surface phases in a metal/semiconductor epitaxy, probed in situ during growth by surface-sensitive techniques such as AES, LEED, EELS, XPS, ultraviolet photoelectron spectroscopy (UPS), scanning tunneling microscopy (STM), etc.

The study of the adsorption of Group V metal antimony on single-crystal silicon surfaces is being intensely pursued to understand the mechanisms underlying several technologically important issues, such as surfactant-mediated Ge/Si heteroepitaxy [3,4] and δ-doped structures [1,2]. The extra valence electron of Sb adatoms on Si allows various ways to minimize the number of surface dangling bonds, which makes it an interesting candidate to study the effect of the growth kinetics. Most of such studies have concentrated on the adsorption of Sb on Si substrates held at high temperatures [5]. Among the Si surfaces, the (111) surface has attracted enormous scientific interest owing to its complicated reconstruction. The 7×7 reconstruction of the Si(111) substrate has been explained by the dimer-adatom-stacking fault (DAS) model [6], which shows a quasi-continuous distribution of states within the bulk band-gap of Si. The (7×7) unit cell consists of two triangular (1×1) subunits with faulted and unfaulted stacking, respectively. These subunits are bound by dimer-row domain walls, which intersect to produce the corner holes. This rest-adatom double layer is capped by Si adatoms. High-resolution electron energy loss spectroscopy (HREELS) and angle-resolved ultraviolet photoelectron spectroscopy (ARUPS) studies [7,8] have shown that some surface states lying close to the Fermi level disperse near the zone boundary and cross the Fermi level, resulting in a metallic character of the Si(111)-7×7 reconstruction. A large amount of work has already been reported in the literature especially for Sb adsorption on Si(111)-7×7 surface. The $(\sqrt{3} \times \sqrt{3} - R30°)$ structure obtained at a substrate temperature of ~650 °C, where only a monolayer that sticks on the surface [9–11] has been widely studied. The $\sqrt{3} \times \sqrt{3} - R30°$ [written as $(\sqrt{3} \times \sqrt{3})$ below] at 1.0 monolayer (ML), d(2×1) at 0.8 ML, and $5\sqrt{3} \times 5\sqrt{3}$–R30° [as $(5\sqrt{3} \times 5\sqrt{3})$ below] at 0.6 ML phases obtained at high temperatures have been reported earlier by LEED studies [12]. However, with the advent of the high-resolution STM, the $(\sqrt{3} \times \sqrt{3})$ at 0.33 ML was observed [13], and a detailed atomistic view of the structures, especially of the $(5\sqrt{3} \times 5\sqrt{3})$ phase at 0.6 ML, emerged [14,15].

The growth kinetics of a metal layer on a reconstructed semiconductor surface has displayed the potential to enable the tuning of interfacial electronic properties. Our previous studies on Ag/Si(111), Ag/Si(001), and Mn/Si(111) [16–18] have prompted us to revisit the Sb/Si(111) interface formation by parametric control. With this goal in view and to understand the role of kinetics and the substrate reconstruction on growth modes and superstructural phases, we have undertaken here the studies of the Sb/Si(111) interface formation at RT at low deposition rates and its thermal desorption in extremely good ultrahigh vacuum (UHV) conditions. The RT adsorption studies result in a layer-by-layer growth of Sb without disturbing the substrate reconstruction up to a critical coverage where a phase transition that influences the electronic properties is observed. Thermal annealing studies provide evidence for several epitaxial rearrangements as the Sb coverage is reduced.

EXPERIMENTAL

The experiments are performed in situ in two UHV chambers at a base pressure of 3×10^{-11} torr. In one chamber with a hemi-spherical sector analyzer (HSA) Mg K_α (1253.6 eV) source and 0–5 kV electron gun for XPS and AES, respectively, are housed, while the other chamber has a cylindrical mirror analyzer (CMA) enabling AES, EELS, and LEED (using 4-grid electron optics) studies. The analyzers are a 0.18 % resolution CMA for AES and EELS, and a 25 meV resolution HSA for XPS, respectively. AES is used as a common technique to ensure compatibility of measurements. The sample is a rectangular piece $(12 \times 10$ mm) cut from a Si(111) wafer (p-type of resistivity of 100 ohm-cm) which is cleaned by a modified Shiraki process [19] to remove the hydrocarbons and form a thin SiO_2 epilayer before being introduced into the UHV chambers. The sample heating is accomplished by a combination of radiative, resistive, and electron-bombardment heating. The sample is flashed in vacuum at

1200 °C for several seconds and cooled gradually to RT to obtain a very clean (7 × 7) surface, as ascertained by AES and LEED. The temperature is measured with an error of ±20 °C by a calibrated W-Re thermocouple and an optical pyrometer. We report here studies using an Sb flux rate of 0.03 ML/min from a home-made Ta-Knudsen cell, at different substrate temperatures (1.0 ML is defined as the density of a bulk truncated Si(111) surface, which is 7.85×10^{14} atoms/cm^2). Thorough degassing and low sublimation temperature of Sb ensures that the base pressure remains below 8×10^{-10} torr even during Sb adsorption. Thermal stability studies are done by annealing the sample to the desired temperature for 2 min and cooling it to RT before making AES, LEED, and EELS measurements.

RESULTS AND DISCUSSION

Room-temperature adsorption

It is known that thicker layers of Sb on Si, which can be of great technological relevance, can be formed at RT [20,21]. Surprisingly, studies of the initial stages of the Sb/Si interface formation at RT have been almost negligible, owing to the perception of lack of superstructural phases. After the pioneering work of Metzger and Allen [22], who reported epitaxial (1 × 1) growth of Sb on Si(111), the other significant work at RT Sb adsorption has been by Cuberes et al. [23], who, however, report disruption of the (7 × 7) substrate structure even by depositing 0.25 ML of Sb, resulting in a rough morphology that promotes 3D island formation. As Sb of constant flux is exposed to the clean Si(111)-7 × 7 surface, the uptake is monitored by a series of Sb 3d core-level spectra. The changes observed map the interfacial growth and highlight the mechanisms of the interface formation. However, in the Si(2p) spectra (not shown), the changes are observed only in intensity but not in the peak positions and fwhm. This can be attributed to the relatively large attenuation length of the Si(2p) XPS electrons in the Sb overlayer, and, thus, the intensity information is coming predominantly from Si atoms that do not participate in the interface formation.

Figure 1 shows the uptake curve for Sb adsorption on the clean Si substrate, which shows a sharp (7 × 7) LEED pattern. The probability of inelastic scattering for the characteristic electron shows an exponential behavior with the overlayer thickness and is utilized to monitor the overlayer, owing to the attenuation of electrons originating from the lower layers. This plot, of the intensity ratio of the adsorbate (Sb 3d) and substrate (Si 2p) XPS core level spectra as a function of time of adsorption, allows us to follow the adsorption kinetics [24]. The graph shows a linear increase in the Sb/Si ratio up to about 30 min and then a change in the slope. We have identified the break point by the procedure adopted by Stampanoni et al. [25], which yields the dotted curve shown in the figure. The curve shows the sum of

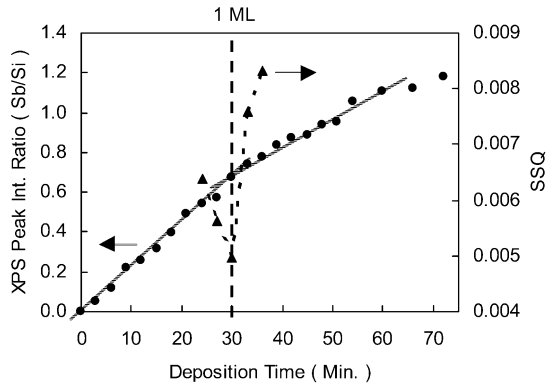

Fig. 1 Uptake curve of the Sb($3d_{5/2}$)/Si(2p) intensity ratio as a function of Sb deposition time (in minutes). Also shown by the dotted curve is the sum of squares of errors (SSQ) to assist in determining the 1.0 ML break at 30 min.

squares of errors (SSQ) in the least-square fits of a set of two straight lines near the break point. The minimum of the SSQ identifies the break point. The linear increase and the sharp points of change in slope shows that Sb adsorption follows Frank van der Merwe (FM) (layer-by-layer) growth mode. FM growth for Sb on Si has been reported earlier [22] with the first break in slope yielding a calibration for 1.0 ML. From the break point, it is inferred that we have a deposition rate of 0.03 ML/min. Nontransition-metal adatoms generally tend to be very mobile and so are expected to form small metallic 3D islands. However, in our case, it is clear that at the deposition rate adopted (0.03 ML/min) we can form several epitaxial layers, at RT, determined by the kinetics of growth. This coverage is also confirmed by finding the Sb(MNN)/Si(LVV) Auger ratio that is obtained by adsorbing Sb onto a substrate heated to 650 °C, which results in the well-known $\sqrt{3} \times \sqrt{3}$ LEED pattern [5,9] with 1.0 ML Sb.

Curves a and b of Fig. 2 are derived from the Sb 3d spectra, after suitable background subtraction and deconvolution into Gaussian components. Curve 2a shows the positions of the Sb $3d_{5/2}$ peak as a function of Sb coverage. The peak remains unchanged at 528.3 eV almost up to a coverage of 1.0 ML and then suddenly shifts to 529.1 eV, showing a shift of 0.8 eV. After 1.0 ML, the peak position decreases monotonically with the coverage up to 2.5 ML, and, therefore, the shift (which was 0.8 eV at 1.0 ML) also decreases by 0.4 eV to a value of 0.4 eV at 2.5 ML. Similar behavior is observed for the Sb $3d_{3/2}$ transition. The shifts in the core-level peak positions in metal/semiconductor interfaces are generally attributed either to formation of Schottky barrier owing to band-bending at the substrate surface or to a chemical interaction between the adsorbate and the substrate. The chemical interaction is highly unlikely at these temperatures for this system, as has been established by several earlier works [26]. Further, the formation of a diffuse interface or a compound formation should have been reflected in the uptake curve of Fig. 1. Usually, the Schottky barrier formation evolves continuously with metal coverages up to a saturation value if the substrate surface is of semiconducting nature. However, it is intriguing that in our case, the Sb 3d core level peaks do not undergo any shift in position in the submonolayer regime, while at about 1.0 ML, there is an abrupt shift by about 0.8 eV. The observation of the flat-band up to 1.0 ML can be attributed to the persistence of metallic nature of the (7×7) structure of the substrate up to this coverage. It is well known that the (7×7) reconstruction leaves the Si(111) surface with metallic nature [27]. Earlier studies on well-ordered (7×7) structures have shown a sharp Fermi edge, and in HREELS, the broad and intense background observed is attributed to a continuum of electronic transitions between continuously distributed surface states [7]. In ARUPS studies [8], at least three different peaks are reported above and below the upper valence band edge, which do not show significant dispersion in the (1×1) Brillouin zone. The surface state bound at about –0.25 eV shows some dispersion near the zone boundary and crosses the Fermi level. Inverse photoemission

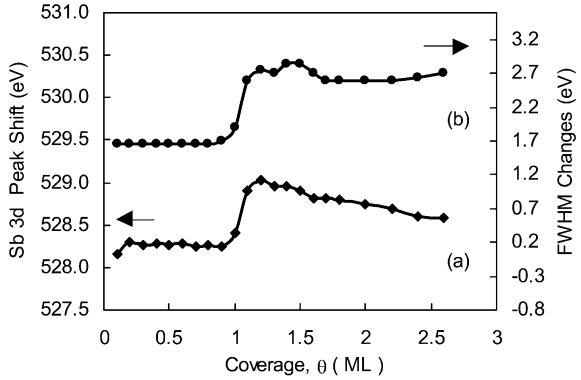

Fig. 2 (a) Shows changes in the Sb $3d_{5/2}$ peak position as a function of Sb coverage at RT. (b) Shows dependence of the fwhm of Sb $3d_{5/2}$ peak on Sb coverage at RT.

experiments also indicate a continuous distribution of empty states in the upper half of the gap with two maxima slightly above the conduction band edge [28]. The density and dispersion of the occupied and unoccupied states may be responsible for the metallic character of the surface. Thus, it appears that at the deposition rate chosen, Sb 2D clusters keep growing up to 1.0 ML, with the metallic nature of (7×7) reconstruction of the Si substrate intact.

The sudden change in the peak position by 0.8 eV at 1.0 ML Sb coverage is interesting. Since we have disregarded the formation of an interfacial compound, we attribute the shift to the formation of a Schottky barrier. The Schottky–Mott relation gives the barrier height of about 0.4 eV for Sb/Si(111)-7×7 interface. The presence of interface states shifts the charge neutrality level (φ_0) below the Fermi energy (E_f). This means that the width of the depletion region and barrier height (φ_b) will be increased, pulling φ_0 up toward E_f [29]. Therefore, the presence of interfacial states might have contributed to the increased barrier height of 0.8 eV than that calculated by a simple Schottky–Mott relation. The formation of the barrier at exactly 1.0 ML suggests that the substrate surface ceases to have the metallic character at this coverage. This abruptness can be attributed to two plausible reasons, which may be mutually competing. Kahn and Stiles [30] have observed such a delayed onset of the barrier formation for adsorption made at low temperatures. They attribute their results to the smallness of the cluster sizes at submonolayer coverages, where the clusters do not form a metallic character. If we assume that this mechanism plays a role in our studies because of the abrupt nature of the change, then it cannot explain completely the present observations unless the substrate surface is semiconducting. The new surface semiconducting phase and the corresponding interface states create a barrier of 0.8 eV. However, it is interesting to note that for coverages greater than 1.0 ML, the shift of peak position (which was 0.8 eV at 1.0 ML) decreases by 0.4 eV to a value of 0.4 eV at 2.5 ML. It is probable that the increased coverage of Sb quenches some of the surface states, thus shifting the neutrality level towards E_f so as to approach the Schottky–Mott value of φ_b.

Figure 2b shows the change in fwhm of the Sb $3d_{5/2}$ as a function of Sb coverage. The fwhm value also remains unchanged almost up to 1.0 ML. The fwhm measured to be ~1.6 eV suddenly assumes a value of ~2.6 eV at the critical coverage of 1.0 ML, suggesting an increased width of the transition level depending on the nature of the interface. Such a coverage dependence of the peak width is reported earlier also in the literature [30,31]. This has been attributed to the formation of isolated metallic clusters at lower coverages, which after a critical thickness form the features typical of metallic Sb owing to s-d hybridization, which can also be applied to view our results. As discussed earlier, in the submonolayer regime, we can understand the flat-band and the relatively narrow peak widths owing to the premetallic dimensions of the Sb clusters. The sudden change in the Sb 3d peak width at 1.0 ML can also suggest an abrupt coalescence of Sb 2D clusters to form the metallic overlayer. The similarity of our results with the low-temperature studies reported above [30] can be due to the adsorption kinetics that can result in rearrangements of atoms in the superstructure with different energetics.

Figure 3 shows an interesting coverage dependence of the anisotropy of the intensities of the Sb core-level spin-orbit split peaks of $3d_{3/2}$ and $3d_{5/2}$ transitions. The ratio of the intensities, which is about 0.82 at a coverage of 0.1 ML, monotonically decreases with increasing Sb coverage and attains a saturation value of 0.67 at the critical coverage of 1.0 ML and remains unchanged for higher coverages. This again highlights the criticality of 1.0 ML and also the absence of any chemical interaction for compound formation. It has been argued in the past, that such anisotropic changes observed in synchrotron X-ray photoelectron spectroscopy (SXPS) are due to the rapid variations in the cross-sections around Cooper minima, which change the radial matrix elements and phase-shift substantially, even for a small difference in the final state energies of $3d_{5/2}$ and $3d_{3/2}$ [32]. In our experiments, we have used conventional Mg K_α radiation with $h\nu$ = 1253.6 eV, which suggests that in this energy regime, such small kinetic energy changes have minimal cross-section differences so that such a process can be discounted. X-ray photoelectron diffraction (XPD) studies have demonstrated this anisotropy as a manifestation of the inherent difference in the photoelectron wave functions of the two spin-orbit components, ruling out significant interference effects [33]. As the Sb adsorption proceeds in the submonolayer regime where

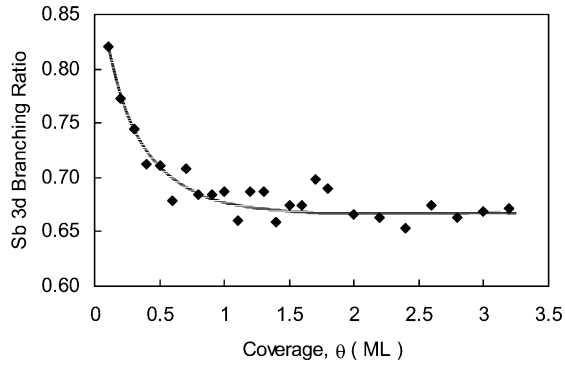

Fig. 3 Branching ratio of the intensities of the Sb $3d_{3/2}$ and $3d_{5/2}$ core-levels as a function of Sb coverage at RT.

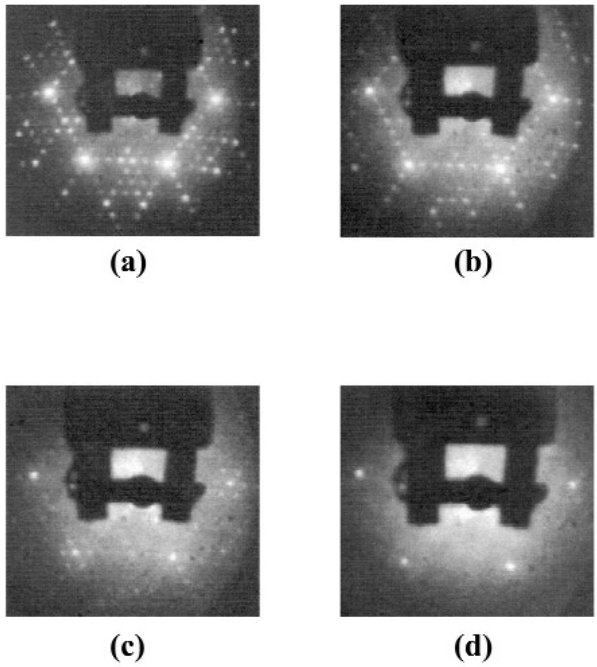

Fig. 4 LEED patterns (at 53 eV) obtained for several Sb coverages adsorbed at RT onto Si(111)-7 × 7 surface. (a) Clean Si(111)-7 × 7, (b) δ(7 × 7) at 0.2 ML, (c) δ(7 × 7) at 0.6 ML, and (d) 1 × 1 at 1.1 ML.

the underlying (7 × 7) structure of the substrate remains intact up to 1.0 ML, the monotonic decrease in the anisotropy of the spin-orbit split peaks may be related to the increasing size of the 2D clusters.

To distinguish the effect of metal-to-semiconductor phase transition, and the lack of metallicity in small 2D clusters, we have performed LEED studies. Figure 4 shows some representative LEED patterns obtained at 53 eV, at different coverages of Sb adsorption onto (7 × 7) reconstructed Si(111) surface held at RT. Figure 4a shows the typical LEED pattern for the clean Si(111) surface, which manifests as the (7 × 7) surface reconstruction with six sharp $1/7^{th}$ fractional order spots between the intense hexagonal integral order spots. With the adsorption of submonolayer quantities of Sb, the changes that occur in the LEED pattern are monitored. Figure 4b is the LEED pattern at 0.2 ML, which shows that

the fractional spots inside the (1 × 1) hexagon have vanished, while those along the adjacent integral spots prevail. Similarly modified (7 × 7) LEED has also been reported earlier by Metzger and Allen [22]. With further increase in coverage, only the fractional order spots around the integral order spots persist as in Fig. 4c for a coverage of 0.6 ML. Increasing further the coverage to values above 1.1 ML, the LEED shows a sharp (1 × 1) structure, shown in Fig. 4d. Such modified (7 × 7) structures for H [34], Li [35], and Ag adsorption [16] on Si(111) have been identified as δ(7 × 7) [5,16], and, thus, we attribute our LEED also to this structure in the submonolayer coverage regime. To understand the evolution of this phase, we have plotted dependence of the intensity ratio of the integral and fractional order LEED spots in Fig. 5 on the Sb coverage. It is clear from the graph that the ratio increases up to a coverage of about 0.4 ML and decreases for coverages above 0.5 ML. At a coverage of about 1.0 ML, the intensity ratio decreases to a very low value ($1/10^{th}$ the maximum value), where only a (1 × 1) LEED is observed. This suggests that the adsorption of Sb does not disturb the underlying (7 × 7) substrate for submonolayer Sb coverages at this low deposition rate. However, at 1.0 ML, the (7 × 7) changes to the (1 × 1) phase.

To look for changes in the electronic structure of this system by monitoring the single-electron transitions and loss to collective electron oscillations, we have performed EELS experiments with an

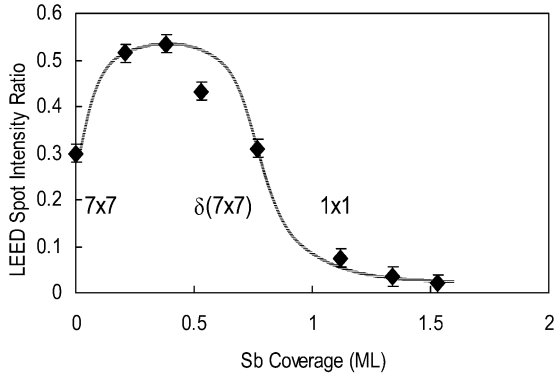

Fig. 5 Intensity ratio of fractional to the integral order LEED spots, obtained for various Sb coverages, is shown along with the unit cell symmetry observed.

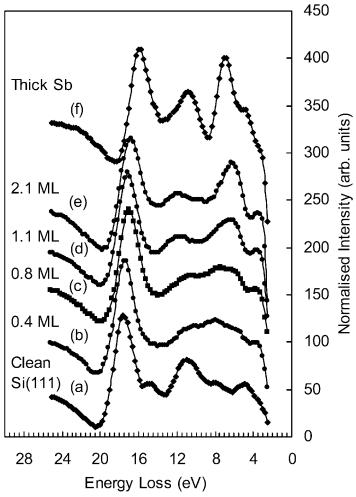

Fig. 6 EELS spectra obtained with primary beam energy (E_p) of 250 eV, at various stages of Sb adsorption at RT.

incident primary beam energy (E_p) of 250 eV. The EELS results are shown in Fig. 6 for clean Si surface and that adsorbed with various Sb coverages. The clean Si(111)-(7 × 7) surface results in the typical pattern as reported earlier [36,37]. The dominant peak at 17.5 eV is due to loss to bulk plasmon, while the peak at 11.0 eV is attributed to the surface plasmon loss. The peaks at 14.5 eV and 8.0 eV are attributed to surface states, and the 4.7 eV peak has been associated with interband transitions at 3.5 and 5.0 eV (Fig. 6a). Now, as the Sb coverage increases, the surface plasmon peak diminishes and only a broad hump is observed in the 5 to 13 eV range as shown in curve Fig. 6b for a coverage of 0.4 ML. As the coverage increases further and attains a very thick Sb overlayer, the bulk plasmon at 17.5 eV monotonically decreases to a value of 16 eV, the Sb bulk plasmon value (Fig. 6f). However, the surface plasmon peak begins to reform at about 0.5 ML, attains a maximum value of 11.7 eV at about 1.0 ML (Fig. 6d) and then decreases monotonically toward the Sb surface plasmon loss value of 11.0 eV. Comparing with the LEED observations, in the region where the δ(7 × 7) structure is formed, the interface plasmon loss appears at 0.4 ML and then attains a maximum value when the (7 × 7) phase is still persistent. After the surface phase becomes (1 × 1), then the surface plasmon loss value for Sb takes over, attaining the bulk value of 11.0 eV for very thick Sb overlayer.

Consolidating the XPS, AES, EELS, and LEED results, it appears that the substrate surface-phase change is the responsible factor for the changes that occur at a critical coverage of 1.0 ML. We postulate a plausible mechanism of the Sb-induced metal-to-semiconductor phase transition of the Si(111) surface. As explained earlier, we recall the well-established DAS model of the (7 × 7) reconstruction. At submonolayer coverages, Sb atoms initially occupy the (1 × 1) sites of the faulted and unfaulted triangular subunits, between and above the Si atoms, keeping the (7 × 7) structure unaltered. As adsorption proceeds, close to 1.0 ML, the Sb adatoms occupy positions on the dimer rows to initiate the shifting of charges from the substrate atoms to the adsorbates. This results in a (7 × 7) to (1 × 1) phase transition due to the filling up of the corner holes with the Si adatoms, under a Sb monolayer. The absence of Si adatoms in the (1 × 1) phase removes the –0.25 eV surface state and consequently renders the substrate semiconducting.

High-temperature annealing

As noted earlier, several surface phases such as the (√3 × √3) at 1.0 ML, d(2 × 1) at 0.8 ML, (5√3 × 5√3) at 0.6 ML and a (√3 × √3) at 0.33 ML have been reported in earlier studies. To understand the mechanism of phase changes and the thermal stability of the system, the residual composition during desorption of the RT deposited films is studied by AES as depicted in Fig. 7 for several

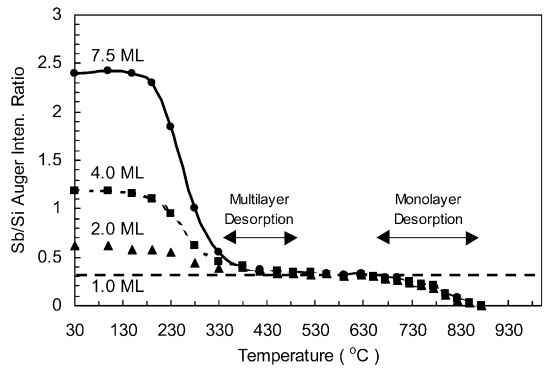

Fig. 7 Shows residual Sb/Si ratio after annealing the substrate for 2 min at each temperature, for various initial Sb coverages adsorbed at RT. The temperature ranges shown (double-sided arrows) for multilayer and monolayer desorption are taken from ref. [22].

coverages of Sb deposited at RT. The figure shows the Sb(MNN)/Si(LVV) Auger ratio as a function of annealing temperature. Also shown in the figure are temperature regions (double-sided arrows in Fig. 7), borrowed from the thermal desorption studies of Metzger and Allen [22], to indicate the desorption temperatures of Sb from the surface. These temperature ranges (350–480 °C and 650–880 °C) correspond to multilayer and monolayer desorption with desorption energies estimated to be 1.49 eV and 2.46 eV, respectively. In the present study, it is clear that at temperatures below the desorption temperatures (in the range 180–350 °C), the Sb/Si Auger ratio decreases almost to a value of 1.0 ML Sb coverage (corresponding to Sb/Si ratio of ~0.32). This indicates that at these sub-desorption temperatures, the Sb adatoms could be agglomerating into large islands on top of a stable Sb monolayer. We estimate the activation energy required for this thermally induced agglomerating process to be about 0.2 eV, assuming Arrhenius form of behavior. Thus, even small changes in the kinetics of growth can induce 3D island growth (which has been reported earlier [23]) of Sb on Si(111) at RT.

Figure 8 shows the LEED pattern obtained at various stages of the desorption process. The (1×1) long-range ordering of the room temperature deposited 1.1 ML sample (Fig. 8a) annealed to ~780 °C gives an Auger ratio corresponding to 0.4 ML of Sb. At this coverage, the LEED pattern shows a (5×5) symmetry (Fig. 8b). This stable phase occurs between the earlier known $(5\sqrt{3} \times 5\sqrt{3})$ at 0.6 ML and the $(\sqrt{3} \times \sqrt{3})$ at 0.33 ML phases. Upon further annealing to 800 °C, the already reported 0.33 ML $(\sqrt{3} \times \sqrt{3})$ phase (Fig. 8c) is observed, although the $\sqrt{3}$ spots are relatively weak. At a temperature of ~820 °C, the Sb coverage reduces to 0.2 ML. At this coverage, we see fractional order spots only around the integral spots, however they are positioned to suggest a $(5\sqrt{3} \times 5\sqrt{3})$ order (Fig. 8d). On further annealing, after going through a (7×7)-Sb phase, the clean (7×7)-Si pattern reappears above 900 °C. The (5×5) at 0.4 ML and the $(5\sqrt{3} \times 5\sqrt{3})$ at 0.2 ML are novel phases observed by us for the first time. It is interesting to note that we do not observe the $(\sqrt{3} \times \sqrt{3})$ at 1.0 ML and $(5\sqrt{3} \times 5\sqrt{3})$ at 0.6 ML phases during residual thermal desorption, which are, however, observed when we deposit

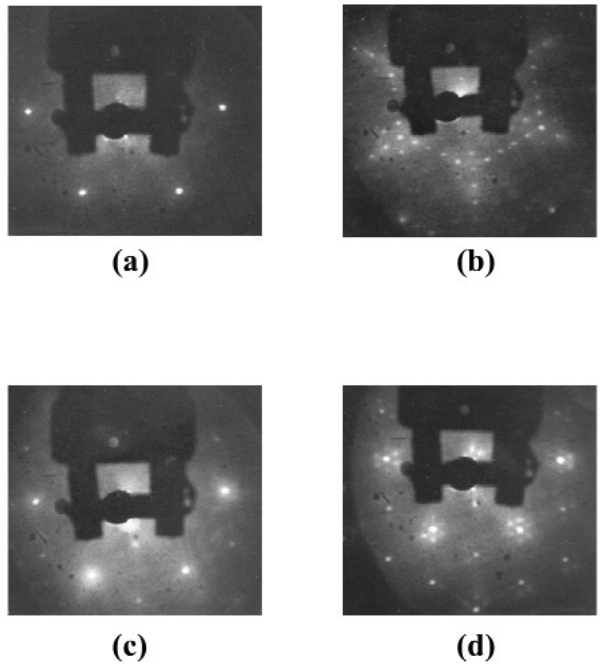

Fig. 8 LEED pattern obtained during various stages of the desorption process for several residual Sb coverages: (a) (1×1) at 1.1 ML (at 53 eV); (b) (5×5) at 0.4 ML (at 53 eV); (c) $(\sqrt{3} \times \sqrt{3} - R30°)$ at 0.33 ML (at 53 eV); and (d) $(5\sqrt{3} \times 5\sqrt{3} - R30°)$ at 0.2 ML (at 63 eV).

Sb onto Si substrate held at the respective temperatures. After further studies by STM, photoelectron spectroscopy (PES), etc. the actual atomic positions in these novel phases can be determined. It will be then interesting to understand why some phases are seen during desorption, while others are excluded from the desorption route. Also, it appears that between integral reconstruction phases, the $\sqrt{3}$ type of phases exist, suggesting that the rearrangement of atoms in the faulted and unfaulted halves of the (7×7) unit cell, have some memory effects. This aspect needs to be probed further.

CONCLUSIONS

We have reported extensive structural studies using conventional surface sensitive techniques to monitor the interface states elucidating the role of kinetics in the Sb/Si(111) interface formation. We also report the studies of the RT adsorption of Sb on (7×7) reconstructed Si(111) surface in extremely good UHV conditions and at very slow deposition rates. Under these conditions, it is observed that the submonolayer coverage Sb adatoms reside at preferential sites on the Si surface without disturbing the (7×7) substrate reconstruction, forming an interface state of $\delta(7 \times 7)$ growing in the Frank van der Merwe mode. As the coverage attains a value of 1.0 ML, the changes in XPS, LEED, AES, and EELS are attributed to the metallic (7×7) substrate phase transforming to a semiconducting (1×1) surface phase, causing an abrupt band-bending resulting in the formation of a Schottky barrier of height 0.8 eV. After 1.0 ML coverage, excess Sb atoms quench some of the surface states and relax the band-bending partially, causing a gradual decrease of Schottky barrier height tending toward the Schottky–Mott value of 0.4 eV. Annealing the RT deposited Sb/Si system shows for the first time that multilayer Sb agglomerates on a stable monolayer before desorbing around 420 °C. However, the first monolayer desorbs at much higher temperatures around 850 °C. The smallness of the magnitude of the energy required (0.2 eV) for island agglomeration suggests that even subtle changes in growth conditions can induce the overlayer to grow epitaxially or form 3D islands and disrupt the substrate. For RT adsorbed system, along with the already reported (1×1), $\delta(7 \times 7)$ and 0.33 ML $(\sqrt{3} \times \sqrt{3})$ phases, we have also observed two novel superstructural surface phases viz., 0.4 ML (5×5) and 0.2 ML $(5\sqrt{3} \times 5\sqrt{3})$. These novel structures, which are stable at higher temperatures, suggest their potential utility in solid-phase epitaxy for the formation of devices like the δ-doped semiconductors that exploit the anomalous properties at nanodimensions. Another interesting potential of the two novel phases, which occur at interfacial coverage regions of other earlier known phases [like $(\sqrt{3} \times \sqrt{3})$ at 0.33 and 1.0 ML, $d(2 \times 1)$ at 0.8 ML, and $(5\sqrt{3} \times 5\sqrt{3})$ at 0.6 ML], can be in understanding the mechanisms for the sequence of surface-phase transformations in this technologically important interface.

ACKNOWLEDGMENTS

The authors gratefully acknowledge the support and encouragement of Director, National Physical Laboratory. Special thanks are due to the Department of Science and Technology, New Delhi, for the financial assistance.

REFERENCES

1. H. J. Gossmann and E. F. Schubert. *Crit. Rev. Solid State Mater. Sci.* **18** (1), 1 (1993) (and references therein).
2. H. P. Zeindl, T. Wegehaupt, I. Eisele, H. Oppolzer, H. Reisinger, G. Tempel, F. Koch. *Appl. Phys. Lett.* **50**, 1164 (1987).
3. M. Horn-von Hoegen, F. K. LeGoues, M. Copel, M. C. Reuter, R. M. Tromp. *Phys. Rev. Lett.* **67**, 1130 (1991).
4. M. I. Larsson, W.-X. Ni, K. Joelsson, G. V. Hansson. *Appl. Phys. Lett.* **65**, 1409 (1994).
5. V. G. Lifshits, A. A. Saranin, A. V. Zotov. *Surface Phases on Silicon*, Wiley, New York (1994).

6. K. Takayanagi, Y. Tanishiro, M. Takahashi, S. Takahashi. *Surf. Sci.* **164**, 367 (1985).
7. G. V. Hansson, R. I. G. Uhrberg, S. A. Flodström. *J. Vac. Sci. Technol.* **16**, 1287 (1979).
8. P. Martensson, W. X. Ni, G. V. Hansson, J. M. Nicholls, B. Reihl. *Phys. Rev. B* **36**, 5974 (1987).
9. T. Abukawa, C.-Y. Park, S. Kono. *Surf. Sci.* **201**, L513 (1988).
10. T. Kinoshita, Y. Enta, H. Ohta, Y. Yaegashi, S. Suzuki, S. Kono. *Surf. Sci.* **204**, 405 (1988).
11. C. Kim, D. A. Walko, I. K. Robinson. *Surf. Sci.* **388**, 242 (1997).
12. C.-Y. Park, T. Abukawa, T. Kinoshita, Y. Enta, S. Kono. *Jpn. J. Appl. Phys.* **27**, 147 (1988).
13. H. B. Elswijk, D. Dijkkamp, E. J. Van Loenen. *Phys. Rev. B* **44**, 3802 (1991).
14. K. H. Park, J. S. Ha, W. S. Yun, E. H. Lee. *Phys. Rev. B* **55**, 9267 (1997).
15. A. A. Saranin, A. V. Zotov, V. G. Lifshits, O. Kubo, T. Harada, M. Katayama, K. Oura. *Surf. Sci.* **447**, 15 (2000).
16. S. M. Shivaprasad, Y. Aparna, S. Singh. *Solid State Commun.* **107**, 257 (1998).
17. S. M. Shivaprasad, C. Anandan, S. G. Azatyan, Y. L. Gavriljuk, V. G. Lifshits. *Surf. Sci.* **382**, 258 (1997).
18. S. M. Shivaprasad, T. Abukawa, H. W. Yeom, M. Nakamura, S. Suzuki, S. Sato, K. Sakamoto, T. Sakamoto, S. Kono. *Surf. Sci.* **344**, L1245 (1995).
19. Y. Enta, S. Suzuki, S. Kono, T. Sakamoto. *Phys. Rev. B* **39**, 56 (1989).
20. U. Rossow, U. Frotscher, N. Esser, U. Resh, Th. Müller, W. Richter, D. A. Woolf, R. H. Williams. *Appl. Surf. Sci.* **63**, 35 (1993).
21. R. Hunger, N. Blick, N. Esser, M. Arens, W. Richter, V. Wagner, J. Geurts. *Surf. Sci.* **307/309**, 1061 (1994).
22. R. A. Metzger and F. G. Allen. *Surf. Sci.* **137**, 397 (1984).
23. M. T. Cuberes, H. Ascolani, M. Moreno, J. L. Sacedón. *J. Vac. Sci. Technol. B* **14**, 1655 (1996).
24. C. Argile and G. E. Rhead. *Surf. Sci. Rep.* **10**, 277 (1989).
25. M. Stampanoni, A. Vaterlans, M. Aeschlimann, F. Meier, D. Pescia. *J. Appl. Phys.* **64**, 5321 (1988).
26. M. Tabe and K. Kajiyama. *Jpn. J. Appl. Phys.* **22**, 423 (1983).
27. C. B. Duke. *Chem. Rev.* **96**, 1237 (1996).
28. J. M. Layet, J. Y. Hoarau, H. Lüth, G. Derrien. *Phys. Rev. B* **30**, 7355 (1984).
29. E. H. Rhoderick and R. H. Williams. *Metal Semiconductor Contacts*, p. 16, Clarendon Press, Oxford (1988).
30. K. Stiles and A. Kahn. *Phys. Rev. Lett.* **60**, 440 (1988).
31. Winfried Mönch. *Rep. Prog. Phys.* **53**, 221 (1990).
32. M. T. Seiger, T. Miller, T.-C. Chiang. *Phys. Rev. Lett.* **75**, 2043 (1995).
33. H. W. Yeom, T. Abukawa, Y. Takkakuwa, S. Fujimori, T. Okane, Y. Ogura, T. Miura, S. Sato, A. Kakizaki, S. Kono. *Surf. Sci. Lett.* **395**, L236 (1998).
34. K. Mortensen, D. M. Chen, P. J. Bedrossian, J. A. Golovchenko, F. Besenbacher. *Phys. Rev. B* **43**, 1816 (1991).
35. S. Kohomoto, S. Mizuno, A. Ichimiya. *Appl. Surf. Sci.* **41–42**, 107 (1989).
36. J. E. Rowe and H. Ibach. *Phys. Rev. Lett.* **31**, 102 (1973).
37. J. K. N. Sharma, B. R. Chakraborty, S. M. Shivaprasad, J. Cazaux. *Surf. Sci. Lett.* **193**, L58 (1988).